Ab Initio MO Study on the Periodic Trends in Structures and Energies of Hypervalent Compounds: Four-Coordinated XH_4^- and XF_4^- Anions Containing a Group 15 Central Atom (X = P, As, Sb, Bi)

Jerzy Moc† and Keiji Morokuma*,‡

Institute for Molecular Science, Myodaiji, Okazaki 444, Japan

Received November 17, 1992®

A systematic *ab initio* MO study employing effective core potentials on the central atoms has been carried out to predict C_{2v}, C_{4v}, D_{4h}, and T_d structures and the corresponding energies and stabilities as well as periodic trends in these molecular properties for the series of hypervalent (hypercoordinated) XH_4^- and XF_4^- anions, where X = P, As, Sb, and Bi. The comparative all-electron calculations for the C_{2v} and C_{4v} structures of these species with X = P, As, and Sb were also done. The lowest energy forms for both XH_4^- and XF_4^- were those of C_{2v} symmetry. All $XF_4^-(C_{2v})$ were found to be minima on the SCF potential energy surfaces, whereas the inclusion of electron correlation (MP2) changed the nature of $PH_4^-(C_{2v})$ and $AsH_4^-(C_{2v})$ from unstable transition states (TS) to stable minima. D_{4h} forms of XH_4^- and PF_4^- appeared to be TS's for inversion of the C_{4v} forms; on the other hand, $XH_4^-(C_{4v})$ and $XF_4^-(C_{4v})$ were found themselves to be TS's connecting C_{2v} minima. The energy decomposition analysis was used to clarify the periodic trends in both the $E(C_{4v}) - E(C_{2v})$ energies for XH_4^- and XF_4^- and in the thermodynamic stabilities of these species relative to loss of H^- or F^-.

1. Introduction

The hypervalent[1a] compounds have been an intriguing topic for both *ab initio* molecular orbital theory and experimental studies, because they break (at least seemingly) the octet rule[1b,c] that is established in chemistry. The first theoretical model proposed to rationalize the nature of the hypervalent bond incorporated d-orbital participation in the hybridization scheme.[2] Since then other models have emerged in which the description of the electronic structure of hypervalent species involves the formation of three-center, four-electron bonds,[3a,b] without a large contribution of d atomic orbitals.[3c] For example, the axial(apical) bond in ten-valence-electron, five-coordinated, 10-X-5, species can be described adequately by such a three-center, four-electron model, with the equatorial bonds being "normal" two-center, two-electron bonds. The apical or equatorial preference shown by different ligands in the structures of hypervalent compounds, called sometimes *apicophilicity* or *equatophilicity*, have also been the subject of recent theoretical investigations.[3d,e] Little attention was devoted to comparative studies for hypervalent species containing central atoms X belonging to the same main group of the periodic Table. In recent years, comparative *ab initio* studies on the molecular systems involving central atoms of a given main group have become possible at a reasonable computational cost through the use of pseudopotentials, which can incorporate relativistic effects.[4]

We present here comparative pseudopotential calculations for ten-valence-electron, four-coordinated, 10-X-4, hypervalent anions with formula XH_4^- as well as for their fluorine analogues XF_4^-, where X = P, As, Sb, and Bi. The present work is the first of a series of papers on the systematic *ab initio* study on structures and energies of the closed-shell XH_n and XF_n hypervalent species, where the coordination number n = 4, 5, 6, 7 and the central atoms X are given above.

For X = P, As, and Sb, all-electron (AE) *ab initio* calculations were also carried out to confirm the reliability of the *ab initio* pseudopotential predictions with regard to the nature of some stationary points located and periodic trends revealed (*vide infra*).

The hypervalent second-row hydrides SiH_5^-, PH_4^-, and SH_4 are an isoelectronic, 10-valence-electron, series. The SiH_5^- anion has been observed in the gas phase[5j] and has attracted considerable attention in theoretical studies.[5a-i] The observation of SH_4 and PH_4^- has not yet been reported. In contrast to the large body of *ab initio* calculations concerning the structure and stability of SH_4[6], only very limited theoretical work has been devoted to PH_4^-. From the early pseudopotential calculations of Trinquier et al.,[7] PH_4^- was predicted to have the C_{2v} structure (as suggested

† JSPS Postdoctoral Fellow. Permanent address: Institute of Chemistry, Wroclaw University, F. Joliot-Curie 14, 50–383 Wroclaw, Poland.

‡ Present address: Department of Chemistry, Emory University, Atlanta, GA 30322.

® Abstract published in *Advance ACS Abstracts*, January 1, 1994.

(1) (a) These compounds are also referred to as "hypercoordinated". (b) Lewis, G. N. *J. Am. Chem. Soc.* **1916**, *38*, 762. (c) Langmuir, I. *J. Am. Chem. Soc.* **1916**, *41*, 868.

(2) (a) Pauling, L. *J. Am. Chem. Soc.* **1931**, *53*, 1367. (b) Pauling, L. *The Nature of the Chemical Bond*, 3rd ed.; Cornell University Press: Ithaca, NY, 1960.

(3) (a) Pimentel, G. C. *J. Chem. Phys.* **1951**, *19*, 446. (b) Rundle, R. E. *J. Am. Chem. Soc.* **1963**, *85*, 112. (c) Kutzelnigg, W. *Angew. Chem., Int. Ed. Engl.* **1984**, *23*, 272. (d) Mathieu, S.; Morokuma, K.; Dorigo, A. E. *The 1989 International Chemical Congress of Pacific Basin Societies*; 1989; PHYS590. Mathieu, S.; Morokuma, K. *Annu. Rev., Inst. Mol. Sci.* **1990**, 18. (e) Wasada, H.; Hirao, K. *J. Am. Chem. Soc.* **1992**, *114*, 16.

(4) (a) Barthelat, J. C.; Durand, Ph.; Serafini, A. *Mol. Phys.* **1977**, *33*, 159. (b) Sakai, Y.; Huzinaga, S. *J. Chem. Phys.* **1982**, *76*, 2552. (c) Krauss, M.; Stevens, W. J. *Annu. Rev. Phys. Chem.* **1984**, *35*, 357. (d) Wadt, W. R.; Hay, P. J. *J. Chem. Phys.* **1985**, *82*, 284.

(5) (a) Maitre, P.; Volatron, F.; Hiberty, P. C.; Shaik, S. S. *Inorg. Chem.* **1990**, *29*, 3047. (b) Sini, G.; Ohanessian, G.; Hiberty, P. C.; Shaik, S. S. *J. Am. Chem. Soc.* **1990**, *112*, 1407. (c) Gordon, M. S.; Windus, T. L.; Burggraf, L. W.; Davis, L. P. *J. Am. Chem. Soc.* **1990**, *112*, 7167. (d) Sini, G.; Hiberty, P. C.; Shaik, S. S. *J. Chem. Soc., Chem. Commun.* **1989**, 772. (e) Kalcher, *J. J. Mol. Struct. (THEOCHEM)* **1988**, *44*, 235. (f) Reed, A. E.; Schleyer, P. v. R. *Chem. Phys. Lett.* **1987**, *133*, 553. (g) Brandemark, U.; Siegbahn, P. E. M.; *Theor. Chim. Acta* **1984**, *66*, 233. (h) Wilhite, D. L.; Spialter, L. *J. Am. Chem. Soc.* **1973**, *95*, 2100. (i) Keil, F.; Ahlrichs, R. *Chem. Phys.* **1975**, *8*, 384. (j) Hajdasz, D. J.; Squires, R. R. *J. Am. Chem. Soc.* **1986**, *108*, 3139.

(6) (a) Downs, A. J.; McGrady, G. S.; Barnfield, E. A.; Rankin, D. W. H.; Robertson, H. E.; Boggs, J. E.; Dobbs, K. D. *Inorg. Chem.* **1989**, *28*, 3286. (b) Ewig, C. S.; Van Wazer, J. R. *J. Am. Chem. Soc.* **1989**, *111*, 1552. (c) Eggers, M. D.; Livant, P. D.; McKee, M. L. *J. Mol. Struct. (THEOCHEM)* **1989**, *55*, 69. (d) Yadav, A.; Surjan, P. R.; Poirier, R. A. *J. Mol. Struct. (THEOCHEM)* **1988**, *42*, 297. (e) Yoshioka, Y.; Goddard, J. D.; Schaefer, H. F. III. *J. Chem. Phys.* **1981**, *74*, 1855. (f) Gleiter, R.; Veillard, A. *Chem. Phys. Lett.* **1976**, *37*, 33. (g) Schwenzer, G. M.; Schaefer, H. F. III. *J. Am. Chem. Soc.* **1975**, *97*, 1393.

(7) Trinquier, G.; Daudey, J.-P.; Caruana, G.; Madaule, Y. *J. Am. Chem. Soc.* **1984**, *106*, 4794.

(8) Nguyen, M. T. *J. Mol. Struct. (THEOCHEM)* **1988**, *49*, 23.

(9) Ortiz, J. V. *J. Phys. Chem.* **1990**, *94*, 4762 and references cited therein.

0020-1669/94/1333-0551$04.50/0

by the VSEPR[11] theory) and found to be slightly thermodynamically unstable towards $PH_3 + H^-$ dissociation. The C_{2v} structure of PH_4^- was also studied recently by Ortiz[9] who employed the MP2/6-311++G(d,p) method for geometry optimization and frequency calculations. The electron affinity for the related PH_4 radical has been investigated theoretically[8,9] and was found to be positive.

Apparently, further theoretical studies on PH_4^- are needed to predict the possible existence of this species. In particular, a thorough investigation of its potential energy surface (PES) must be accomplished. Also, we are interested in periodic trends, so similar work for the "heavier" analogues of PH_4^- involving arsenic (AsH_4^-), antimony (SbH_4^-), and bismuth (BiH_4^-) has been addressed. As in the case of PH_4^-, there is no yet experimental evidence for the existence of AsH_4^-, SbH_4^-, and BiH_4^-. To our knowledge, AsH_4^- has been the subject of just one theoretical study already mentioned,[7] where it was found to be stable with respect to $AsH_3 + H^-$.[37] No vibrational analysis was done for the reported C_{2v} structure. We could not find in the literature any previous quantum-chemical calculations on SbH_4^- [37] and BiH_4^-.

Electronegative fluorine atoms can stabilize structures of hypervalent compounds when substituted appropriately.[12] Yet, there is ample experimental evidence for the existence of numerous hypervalent perfluorides.[13] Examples include SiF_6^{2-}, PF_6^-, PF_5, SF_6, ClF_5, and IF_7. That is why the fully fluorine substituted analogues of the XH_4^- hydrides, i.e. PF_4^-, AsF_4^-, SbF_4^-, and BiF_4^- have also been studied in this work. Among the XF_4^- fluorides, only PF_4^- has been the subject of previous theoretical study[10] where its C_{2v} geometry as well as the fluoride affinity for related PF_3 have been found from the SCF calculations.[38,39]

The specific goals of the present theoretical study on the XH_4^- and XF_4^- hypervalent anions are as follows: (i) extensive mapping of their PES's, where, for this purpose, a number of geometrical structures including C_{2v}, C_{4v}, D_{4h}, and T_d symmetries have been optimized and characterized subsequently by a vibrational frequency analysis; (ii) prediction of thermodynamic stabilities of XH_4^- anions relative to the $XH_3 + H^-$ and $XH_2^- + H_2$ decomposition products as well as the thermodynamic stabilities of the XF_4^- anions with respect to the $XF_3 + F^-$ decomposition products; (iii) exploring periodic trends in the Group 15 with respect to the optimized structures and various relative energies (*vide infra*). In an effort to more fully understand the periodic trends revealed, an energy decomposition analysis (EDA) of Morokuma and Kitaura[14] has been carried out for the hypervalent anions studied.

2. Computational Methods

2.1. ECP Calculations. We used the effective-core potentials (ECP) of Wadt and Hay[4d] for P, As, Sb, and Bi atoms with a variety of basis sets described as follows. Basis I: for test calculations, the valence (3s3p2d)/[3s3p2d] basis derived by decontraction of Wadt and Hay[4d] (3s3p) set followed by addition of two sets of d polarization functions[20] was utilized together with the polarized double-ζ (DZP) bases for F and H of the form (9s5p1d)/[3s2p1d] and (4s1p)/[2s1p], respectively.[21] This basis set was also used in the EDA calculations. Basis II: The bulk of the ECP calculations on the hypervalent anions employed basis I augmented with additional diffuse sp functions on the central atoms[23] as well as on the F and H atoms.[21] Basis II was also used in the calculation of the systems relevant to the stabilities of XH_4^- (XF_4^-) relative to $XH_3 + H^-$ ($XF_3 + F^-$) and in the calculation of the systems relevant to the stabilities of XH_4^- with respect to $XH_2^- + H_2$. Basis III: Following the previous experience,[9,29] in the calculation of the T_d structures of XH_4^-, we employed a basis set containing additional diffuse functions. This basis is the same as basis II, except that two additional diffuse sp functions[23] were added on the central atom. Basis IV: Occasionally, the Wadt and

(10) O'Keeffe, M. *J. Am. Chem. Soc.* **1986**, *108*, 4341. A 6-31G(d) basis set supplemented with diffuse p orbital on F was used.
(11) Gillespie, R. J. *Angew. Chem.* **1967**, *79*, 885.
(12) See, e.g.: Ewig, C. S.; Van Wazer, J. R. *J. Am. Chem. Soc.* **1989**, *111*, 4172 and references cited therein.
(13) See: Reed, A. E.; Schleyer, P. v. R. *J. Am. Chem. Soc.* **1990**, *112*, 1434 and references therein.
(14) Morokuma, K.; Kitaura, K. In *Chemical Applications of Atomic and Molecular Electrostatic Potentials*; Politzer, P. P., Truhlar, D. G., Eds.; Plenum Publishing Corp.: New York, 1981.
(15) (a) Dixon, D. A.; Arduengo, A. J. III. *J. Am. Chem. Soc.* **1987**, *109*, 338 and references cited therein. (b) It has been shown[15a] that the XF_3 molecules (X = P, As, Sb) invert through a C_{2v} planar structure in contrast to the XH_3 molecules which invert through the more familiar D_{3h} transition state.
(16) Sakai, Y.; Miyoshi, E. *J. Chem. Phys.* **1988**, *89*, 4452.
(17) Dai, D.; Balasubramanian, K. *J. Chem. Phys.* **1990**, *93*, 1837.
(18) Callomon, J. H.; Hirota, E.; Kuchitsu, K.; Lafferty, W. J.; Maki, A. G.; Pote, C. S. *Structure Data of Free Polyatomic Molecules*; Landolt-Bornstein, New Series, Group II; Springer-Verlag: Berlin, 1976; Vol. 7.
(19) Konaka, S.; Kimura, M. *Bull. Chem. Soc. Jpn.* **1970**, *43*, 1693.
(20) Huzinaga, S.; Andzelm, J.; Klobukowski, M.; Radzio-Andzelm, E.; Sakaki, Y.; Tatewaki, H. *Gaussian Basis Sets for Molecular Calculations*; Elsevier: New York, 1984. Cartesian d-type orbitals were used in the ECP and AE calculations.
(21) Dunning, T. H.; Hay, J. P. In *Modern Theoretical Chemistry*; Schaefer, H. F., III, Ed.; Plenum Press: New York, 1977; Vol. 3, pp 1–27. The d and p polarization exponents used for F and H, respectively, were 0.9 and 0.75. The diffuse sp exponents for the two atoms were taken from ref 25.
(22) (a) Møller, C.; Plesset, M. S. *Phys. Rev.* **1934**, *46*, 618. (b) Pople, J. A.; Binkley, J. S.; Seeger, R. *Int. J. Quantum Chem. Symp.* **1976**, *10*, 1. (c) Krishnan, R.; Frisch, M. J.; Pople, J. A. *J. Chem. Phys.* **1980**, *72*, 4244.
(23) ECP calculations: The single diffuse orbital sp exponents for the central atoms were 0.0357, 0.0306, 0.0240, and 0.0224 for P, As, Sb, and Bi, respectively; the additional diffuse orbital sp exponents for the central atoms (for the $XH_4^-(T_d)$ structures) have been obtained by multiplying the above exponents by 0.3 (see ref 9). AE calculations: In s space, the diffuse exponents were 0.033, 0.031, and 0.024 for P, As, and Sb, respectively; in p space, the corresponding exponents were 0.025, 0.020, and 0.016.
(24) Frisch, M. J.; Pople, J. A.; Binkley, J. S. *J. Chem. Phys.* **1984**, *80*, 3265.
(25) Clark, T.; Chandrasekhar, J.; Spitznagel, G. W.; Schleyer, P. v. R. *J. Comput. Chem.* **1983**, *4*, 294.
(26) Frisch, M. J.; Binkley, J. S.; Schlegel, H. B.; Raghavachari, K.; Melius, C. F.; Martin, R. L.; Stewart, J. J. P.; Bobrowicz, F. W.; Rohlfing, C. M.; Kahn, L. R.; DeFrees, D. J.; Seeger, R.; Whiteside, R. A.; Fox, D. J.; Fluder, E. M.; Pople, J. A. *GAUSSIAN86*, Carnegie-Mellon Quantum Chem istry Publishing Unit: Pittsburgh, PA, 1984. IMS adaptation and modifications were performed by N. Koga, S. Yabushita, K. Sawabe and K. Morokuma. EDA links were written by T. Komatsuzaki.
(27) Frisch, M. J.; Head-Gordon, M.; Schlegel, H. B.; Raghavachari, K.; Binkley, J. S.; Gonzalez, C.; DeFrees, D. J.; Fox, D. J.; Whiteside, R. A.; Seeger, R.; Melius, C. F.; Baker, J.; Martin, R.; Kahn, L. R.; Stewart, J. J. P.; Fluder, E. M.; Topiol, S.; Pople, J. A. *GAUSSIAN88*; Gaussian, Inc.: Pittsburgh, PA, 1988.
(28) Frisch, M. J.; Head-Gordon, M.; Trucks, G. W.; Foresman, J. B.; Schlegel, H. B.; Raghavachari, K.; Robb, M.; Binkley, J. S.; Gonzalez, C.; DeFrees, D. J.; Fox, D. J.; Whiteside, R. A.; Seeger, R.; Melius, C. F.; Baker, J.; Martin, R.; Kahn, L. R.; Stewart, J. J. P.; Topiol, S.; Pople, J. A. *GAUSSIAN 90*; Gaussian, Inc.: Pittsburgh, PA, 1990.
(29) Ortiz, J. V. *J. Chem. Phys.* **1987**, *87*, 3557.
(30) (a) Reed, A. E.; Weinstock, R. B.; Weinhold, F. *J. Chem. Phys.* **1985**, *83*, 735. (b) Foster, J. P.; Weinhold, F. *J. Am. Chem. Soc.* **1980**, *102*, 7211.
(31) In a PTBP structure, a lone pair occupies one of the equatorial positions instead of an X–H (X–F) bond.
(32) Berry, R. S. *J. Chem. Phys.* **1960**, *32*, 933.
(33) Sakaki, S.; Sato, H.; Imai, Y.; Morokuma, K.; Ohkubo, K. *Inorg. Chem.* **1985**, *24*, 4538 and early references cited therein.
(34) Although the natural charges for XH_4^- and XF_4^- were computed using different bases, it has been shown previously (see, e.g., ref 13) that NPA charges are not very sensitive to the basis set.
(35) The RHF/ECP (basis II) geometries of $XH_4^-(C_{2v})$ and $XF_4^-(C_{2v})$ were assumed with the exception of $PH_4^-(C_{2v})$ for which the MP2/ECP (basis II) geometry was used.
(36) The difference between the RHF/ECP values in Table 5 and ΔE values for the hydrides and fluorides in Tables 6 and 7, respectively, is caused by the fact that different basis sets were used for EDA and for computing reaction energies (cf. Computational Methods).
(37) For the theoretical work on the isoelectronic SeH_4 and TeH_4 species, see: Moc, J.; Dorigo, A. E.; Morokuma, K. *Chem. Phys. Lett.* **1993**, *204*, 65 and references cited therein.
(38) The theoretical work on isoelectronic SF_4 includes: (a) Magnusson, E. *J. Am. Chem. Soc.* **1990**, *112*, 7940. (b) Innes, E. A.; Csizmadia, I. G.; Kanada, Y. *J. Mol. Struct. (THEOCHEM)* **1989**, *55*, 1. (c) Magnusson, E.; Schaefer III, H. F. *J. Chem. Phys.* **1985**, *83*, 5721. (d) Pietro, W. J.; Francl, M. M.; Hehre, W. J.; DeFrees, D. J.; Pople, J. A.; Binkley, J. S. *J. Am. Chem. Soc.* **1982**, *104*, 5039. (e) Hay, P. *J. Am. Chem. Soc.* **1977**, *99*, 1003. (f) Oberhammer, H.; Boggs, J. E. *J. Mol. Struct.* **1979**, *56*, 107.
(39) For the theoretical work on the isoelectronic SeF_4 and TeF_4 species, see: Novak, I. *Heteroatom Chemistry* **1992**, *3*, 431.

Table 1. Comparison of the All-Electron and Effective Core Potential *ab Initio* Results for the XH_3 and XF_3 (X = P, As, Sb, Bi) Molecules—RHF Geometries[a]

species	ECP[b]	AE[c]	model pot.[d]	Exp[e]
PH_3	1.409	1.407		1.420
	95.3	95.2		93.3
AsH_3	1.510	1.508		1.511
	94.5	94.3		92.1
SbH_3	1.697	1.707		1.704
	93.8	94.3		91.6
BiH_3	1.759			
	92.5			
PF_3	1.560	1.563		1.570, 1.563
	97.2	97.1		97.8, 96.9
AsF_3	1.683	1.693	1.699	1.704, 1.710
	95.5	95.4	95.5	96.0, 96.0
SbF_3	1.849	1.874	1.885	1.879
	94.3	93.6	94.4	95.0 ± 0.8
BiF_3	1.925			
	94.8			

[a] The first entry is the bond length (in Å), and the second entry is the bond angle (in deg). [b] This work: results of *ab initio* calculations employing effective core potentials on the central atoms in conjunction with basis I. [c] All-electron *ab initio* results.[15] The basis sets used were the following: P(11s7p1d)/[6s4p1d], As(14s11p6d)/[10s8p3d], Sb(15s11p8d)/[10s7p5d], F(9s5p1d)/[3s2p1d], and H(4s1p)/[2s1p] (for AsH_3 and SbH_3, the H basis was (5s1p)/[3s1p]). [d] Results of *ab initio* computations using model potentials on the central atoms and fluorine atoms.[16] The basis sets employed were of valence triple-ζ quality augmented by two d polarization functions on the central atoms, and of valence double-ζ quality augmented by a d polarization function on the F atom. [e] Experimental Values.[19,20]

Hay[4d] (3s3p)/[2s2p] basis on the central atom together with the fluorine (9s5p)/[3s2p] set[21] was employed.

All structures were gradient optimized using mostly RHF wave functions (RHF/ECP level). Stationary points found on the PES's were subjected to frequency analysis in order to determine whether they correspond to local minima (zero imaginary frequencies), transition states (one imaginary frequency), or higher-order saddle points (two or more imaginary frequencies). The RHF/ECP vibrational frequencies were evaluated numerically using analytical gradients. When necessary, the correlation energy was calculated (at the RHF/ECP structures) using the Møller-Plesset perturbation theory[22a] through full fourth-order calculations (MP4)[22c] for the hydrides and through second-order calculations (MP2)[22b] for the fluorides (MPn/ECP level). Occassionally, MP2/ECP geometry optimizations followed by MP2/ECP frequency calculations were carried out. The calculations were accomplished by means of the GAUSSIAN 88[27] and GAUSSIAN 90[28] programs, except for EDA analysis (RHF/ECP), which was carried out with a locally modified version of GAUSSIAN 86.[26]

2.2. AE Calculations. In the AE computations we employed the (433/43), (4333/433/4), and (43333/4333/43) basis sets of Huzinaga et al.[20] for P, As, and Sb, respectively, which were split into the forms (4321/421), (43321/4321/31), and (433321/43321/421), respectively. These split sets were supplemented with two d polarization functions[20] and diffuse s and p functions[23] and used in conjunction with the DZP bases for F and H described above, augmented by diffuse sp functions.[21] Henceforth, we will refer to these basis sets as basis AE. For the hydrides, AE geometry optimizations and subsequent frequency calculations were done at both RHF and MP2 levels, whereas for the fluorides only RHF structure optimizations were carried out. The RHF frequencies were computed analytically, whereas the MP2 frequencies were evaluated numerically using analytical gradients. For the PF_4^- structures, the RHF/6-31+G(d)[24] geometry optimizations were also carried out for purposes of comparison with the RHF/ECP and RHF/basis AE findings.

3. Results

3.1. Testing ECP's for Normal-Valent Molecules. We first tested the performance of the ECP's and basis I with regard to the calculation of structures and energetics of normal-valent molecules. The test molecules were the hydrides XH_3 and fluorides XF_3. The AE study using large basis sets was reported in literature[15] for X = P, As, and Sb, whose results were used here for comparison.

Table 1 presents the AE and ECP C_{3v} geometries of XH_3 and XF_3. Also shown in Table 1 are the available experimental[18,19] values and, for AsF_3 and SbF_3, results of *ab initio* computation[16] employing the model potentials of Sakai and Miyoshi. It is seen from Table 1 that the ECP geometries compare favorably with the AE and experimental structures as well as with the *ab initio* model potential results. The mean absolute deviations of the ECP and AE from the experimental hydride and fluoride bond lengths are 0.013 and 0.007 Å, respectively, and for bond angles the mean absolute deviations from the experimental data are 1.3 and 1.5°, respectively. For the ECP applied to hydrides, the mean absolute deviations of the bond lengths and bond angles from known experimental data are 0.006 Å and 2.2°, respectively, and for the fluorides these values are 0.020 Å and 0.4°, respectively.

Table 2. Comparison of the All-Electron and Effective Core Potential *ab Initio* Results for the XH_3 and XF_3 (X = P, As, Sb, Bi) Molecules—RHF and MP2 Inversion Barriers[a]

		ECP[b]		AE[c]	
species	inversion	RHF	MP2	RHF	MP2
PH_3	$C_{3v} \rightarrow D_{3h} \rightarrow C_{3v}$	37.6	34.7	36.3	35.0
AsH_3		41.9	39.7	42.4	41.3
SbH_3		47.8	44.9	44.8	42.8
BiH_3		63.4	60.5		
PF_3	$C_{3v} \rightarrow C_{2v} \rightarrow C_{3v}$	67.7	52.4	68.4	53.8
AsF_3		57.8	45.7	57.7	46.3
SbF_3		45.4	37.6	46.5	38.7
BiF_3		38.7	33.5		

[a] In kcal/mol. [b] This work: results of *ab initio* calculations employing effective core potentials on the central atoms in conjunction with basis I. [c] All-electron *ab initio* results.[15] The basis sets used were the following: P(13s9p1d)/[6s4p1d], As(14s11p6d)/[10s8p3d], Sb(15s11p8d)/[10s7p5d], F(9s5p1d)/[4s2p1d], and H(4s1p)/[2s1p] (for AsH_3 and SbH_3, the H basis was (5s1p)/[3s1p]).

In Table 2 we compare the ECP and AE inversion barriers of the test molecules as computed at the RHF and MP2 levels (on the RHF geometries).[15] It appears from Table 2 that the ECP method could reproduce the periodic trends found from the AE calculation: the hydride (C_{3v}–D_{3h}–C_{3v}) barriers increase monotonically and the fluoride (C_{3v}–C_{2v}–C_{3v}) barriers decrease monotonically on passing from P to As to Sb. The results shown in Table 2 for AsH_3, SbH_3, and BiH_3 parallel the recent ECP CAS CI findings of Dai and Balasubramanian.[17] In particular, they also found that the inversion barrier of BiH_3 is much larger than those for AsH_3 and SbH_3.[40]

The test calculations indicate that the ECP model used is adequate for the calculation of structures and energies of the normal-valent molecules containing the P, As, Sb, and Bi central atoms.

3.2. RHF/ECP Optimized Structures and Their Vibrational Analysis. C_{2v} Symmetry. Pseudo-trigonal-bipyramidal (PTBP) structures[31] of C_{2v} symmetry (Figures 1 and 2) were predicted to be of lowest energy for both XH_4^- and XF_4^- (X = P, As, Sb, Bi). The C_{2v} structures of the hydrides show remarkably long axial distances, whereas the equatorial distances are virtually the same as those in the corresponding XH_3 molecules (cf. Table 1). For the PTBP structures of the fluorides, the dissimilarity in the

(40) When our paper was being revised the results of recent *ab initio* calculations on the inversion barriers for the group 15 hydrides XH_3 and fluorides XF_3 (X = N, P, As, Sb, Bi)[41] were brought to our attention. The periodic trends in the inversion barriers found[41] for both the PH_3, AsH_3, SbH_3, and BiH_3 series and PF_3, AsF_3, SbF_3, and BiF_3 series are in complete agreement with our results.

(41) Schwerdtfeger, P.; Laakkonen, L. J.; Pyykko, P. *J. Chem. Phys.* **1992**, *96*, 6807 and references cited therein.

(42) Bierbaum, V. Personal communication to N. Matsunaga, 1990.

(43) Matsunaga, N.; Gordon, M. S. Manuscript in preparation. This loosely bound complex of PH_2^- and H_2 lies about 33 kcal/mol below $PH_3 + H^-$ and has essentially the same energy as $PH_2^- + H_2$ at the G1[44] level of theory.

(44) (a) Pople, J. A.; Head-Gordon, M.; Douglas, J. F.; Raghavachari, K.; Curtiss, L. A. *J. Chem. Phys.* **1989**, *90*, 5622. (b) Curtiss, L. A.; Jones, C.; Trucks, G. W.; Raghavachari, K.; Pople, J. A. *J. Chem. Phys.* **1990**, *93*, 2537.

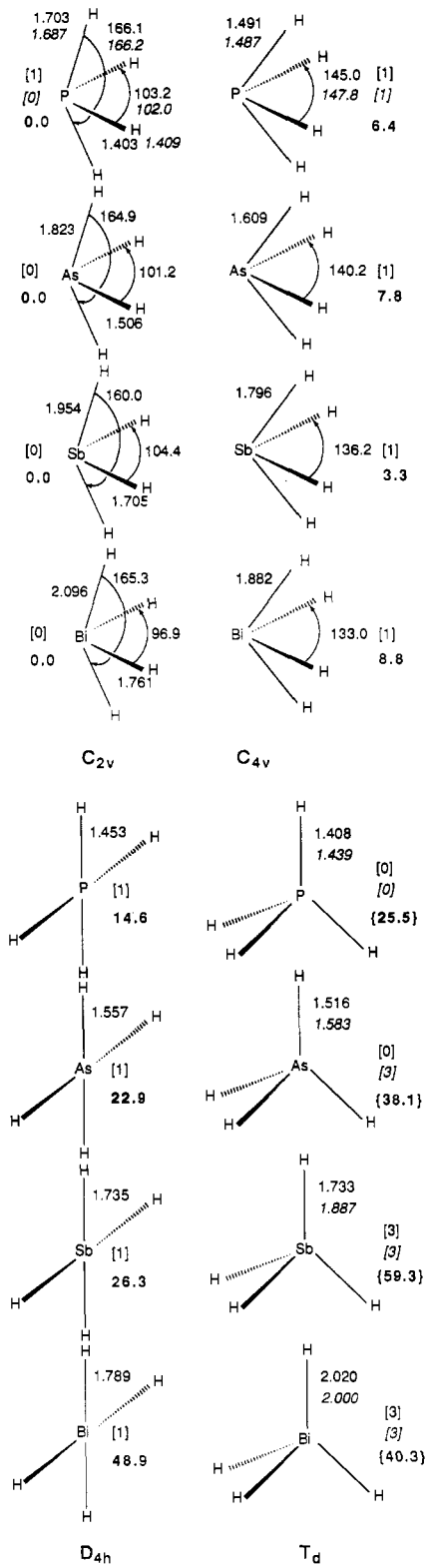

Figure 1. C_{2v}, C_{4v}, D_{4h}, and T_d structures of XH_4^- (X = P, As, Sb, Bi) optimized at the RHF/ECP level with basis II (bond lengths in angstroms; bond angles in degrees). Values shown in boldface correspond to RHF energies relative to the C_{2v} structures (in kcal/mol); the number of associated imaginary frequencies is given in square brackets. Values in italics for the T_d structures, $PH_4^-(C_{2v})$, and $PH_4^-(C_{4v})$ are from the MP2/ECP calculation (basis II). Basis III was employed for the optimization of the T_d structures. The relative energies given in curly brackets were computed with basis III.

X–F bonds (the axial bonds being again longer than the equatorial bonds) is less pronounced than for the hydrides structures. It is also seen from Figures 1 and 2 that the axial HXH(FXF) angles behave irregularly. That is, they decrease in going from X = P to X = As to X = Sb and then increase with X = Bi.

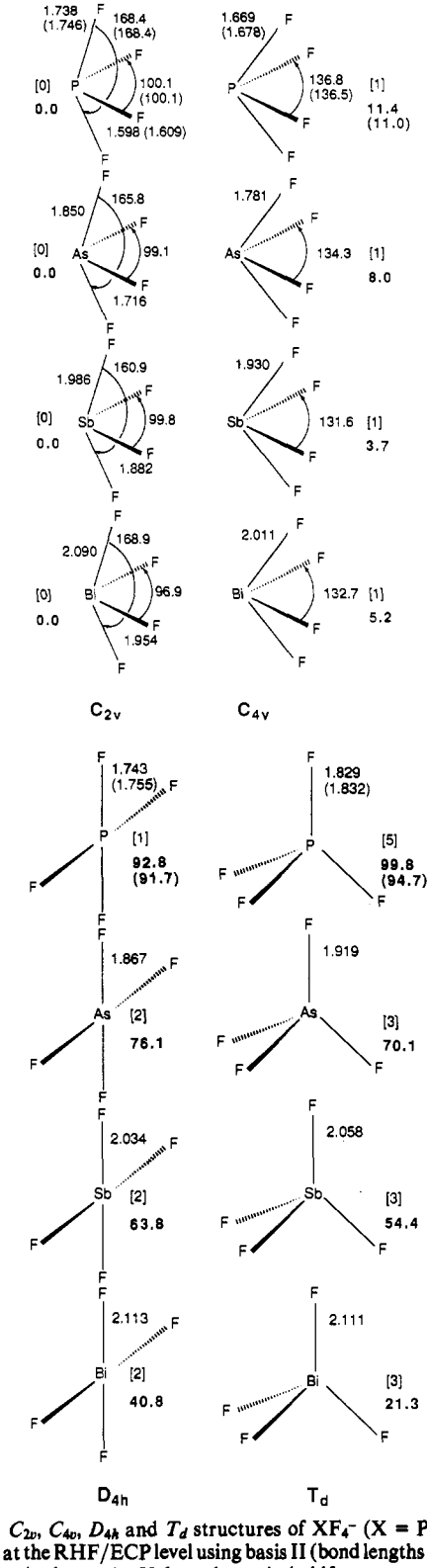

Figure 2. C_{2v}, C_{4v}, D_{4h} and T_d structures of XF_4^- (X = P, As, Sb, Bi) optimized at the RHF/ECP level using basis II (bond lengths in angstroms; bond angles in degrees). Values shown in boldface correspond to RHF energies relative to the C_{2v} structures (in kcal/mol); the number of associated imaginary frequencies is given in square brackets. Values in parentheses for the PF_4^- structures are from the RHF/6-31+G(d) calculation.

The RHF/ECP vibrational analysis shows that the C_{2v} structures of XH_4^- have all real frequencies, except for PH_4^-. A frequency analysis of $PH_4^-(C_{2v})$ indicates that the optimized structure is a local minimum when correlation effects (MP2/ECP) are included (zero imaginary frequencies) but a saddle point with one imaginary frequency for the b_2 vibrational mode at the RHF/ECP level of calculation. This mode leads to dissociation of H^- from the axial position. On the other hand,

Scheme 1. Illustration of Berry-like Pseudorotation for the XL_4^- Species (X = P, As, Sb, Bi; L = H, F) Exchanging the Axial (L1, L2) and Equatorial (L3, L4) Pairs of Ligands Through the C_{4v} Transition State

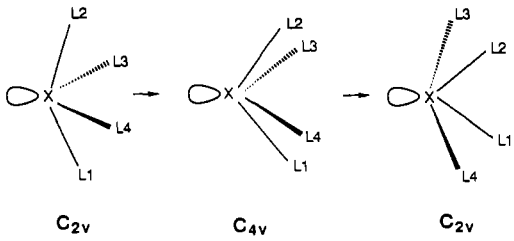

Table 3. MP2 and MP4 Energy Differences between the C_{4v} and C_{2v} Structures and between the D_{4h} and C_{4v} Structures[a]

energy	species	MP4/ECP[b]	MP2/AE[c]	species	MP2/ECP[b]
$E(C_{4v}) - E(C_{2v})$	PH_4^-	4.5	5.0	PF_4^-	10.6
	AsH_4^-	6.1	7.5	AsF_4^-	7.5
	SbH_4^-	2.1	0.6	SbF_4^-	4.0
	BiH_4^-	7.2		BiF_4^-	5.4
$E(D_{4h}) - E(C_{4v})$	PH_4^-	5.2			
	AsH_4^-	11.6			
	SbH_4^-	17.8			
	BiH_4^-	32.6			

[a] In kcal/mol. [b] Calculated using basis II at the RHF/ECP geometries. [c] MP2/basis AE//MP2/basis AE.

the RHF/ECP vibrational analysis indicates that the C_{2v} forms of XF_4^- are all local minima.

***C_{4v}* Symmetry.** For both the XH_4^- and XF_4^- species, the structures of C_{4v} symmetry were found to lie higher in energy than the corresponding C_{2v} forms. The bond angles indicated in Figure 1 for the $XH_4^-(C_{4v})$ geometries decrease monotonically as the size of the central atom increases. The same holds for the analogous angles in the $XF_4^-(C_{4v})$ structures (Figure 2), except for X = Bi. We note that the vertex of pyramids formed by the fluorides is sharper than for the hydride counterparts, because of the central atom lone pair-fluorine lone pairs repulsive interactions.

The RHF/ECP vibrational analysis reveals that the C_{4v} structures of XH_4^- and XF_4^- are all characterized by one imaginary frequency corresponding to a b_2 mode. This mode corresponds to displacement of one pair of the opposed ligands upward and displacement of the second pair of the opposed ligands (in the perpendicular plane) downward. Thus, C_{4v} geometries are transition states (TS) in the exchange of two axial ligands (L_1, L_2) and two equatorial ligands (L_3, L_4) in C_{2v} structures (C_{2v}–C_{4v}–C_{2v} path, Scheme 1). The motion illustrated in Scheme 1 resembles the Berry-like pseudorotation[32] with the equatorially localized lone pair being the pivot "ligand". We note again that a correlated wave function may be needed to characterize correctly the nature of the C_{2v} structures of the XH_4^- species involved in this pseudorotation.

It can be seen from Figures 1 and 2 that the $E(C_{4v}) - E(C_{2v})$ energy differences are rather small: they are within 8.8 and 11.4 kcal/mol (RHF/ECP) for the hydrides and fluorides, respectively. For the hydrides, these energy differences increase in going from X = P to X = As, decrease in going from X = As to X = Sb, and then increase again with X = Bi; for the fluorides, they decrease monotonically in going from X = P to X = As to X = Sb and increase with X = Bi. Inclusion of electron correlation (MPn/ECP, Table 3) does not alter these irregular trends. We will check below the validity of these trends for X = P, As, and Sb through the AE calculations and try to clarify them by EDA.

***D_{4h}* Symmetry.** The D_{4h} structures of XH_4^- are found to be higher in energy than the corresponding C_{4v} geometries. A vibrational analysis (Figure 1) shows that the $XH_4^-(D_{4h})$ structures are all characterized by one imaginary frequency corresponding to an a_{2u} mode. This mode is an inversion mode

Scheme 2. Illustration of the C_{4v}–D_{4h}–C_{4v} Inversion

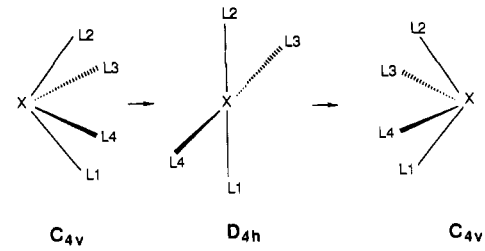

corresponding to displacement toward the C_{4v} geometry. Thus, the D_{4h} structures of XH_4^- are saddle points for inversion of the C_{4v} structures (C_{4v}–D_{4h}–C_{4v} path, Scheme 2). On the other hand, as we already reported, the C_{4v} structures are themselves saddle points connecting two equivalent C_{2v} minima if one follows the direction of the pseudorotation mode (Scheme 1). There must be a change in the sign of force constant from negative to positive for the b_2 mode between the C_{4v} and D_{4h} structure.

The energy differences between the $XH_4^-(D_{4h})$ and $XH_4^-(C_{4v})$ structures increase as the size of the central atom increases, being 8.2(5.2), 15.1(11.6), 23.0(17.8), and 40.1(32.6) kcal/mol for X = P, As, Sb, and Bi, respectively at the RHF/ECP(MP4/ECP) level. This regular periodic behavior can be explained (at least in part) by the fact that the vertex of pyramids of the XH_4^- structures become progressively sharper on passing down the column (Figure 1); therefore, the energy requirement for the C_{4v}–D_{4h} distortion would increase correspondingly.

The $PF_4^-(D_{4h})$ structure (Figure 2) resembles the D_{4h} structures of the hydrides XH_4^-, as it is also a saddle point for the C_{4v}–D_{4h}–C_{4v} inversion (Scheme 2). Substitution of fluorines for hydrogens in PH_4^- to form PF_4^- results in an increase of the inversion barrier, which is 81.4 and 80.7 kcal/mol at RHF/ECP (basis II) and RHF/6-31+G(d), respectively. This is analogous to the PH_3 and PF_3 inversion barriers studied above (cf. Table 2).

Unlike the $PF_4^-(D_{4h})$ structure, the D_{4h} geometries of "heavier" AsF_4^-, SbF_4^-, and BiF_4^- are higher order stationary points having two imaginary frequencies that connect two TS's, each having one imaginary frequency.

***T_d* Symmetry.** Among the hypervalent hydrides studied, PH_4^- is shown to be the only species having a stable T_d structure (Figure 1). A vibrational analysis indicates that $PH_4^-(T_d)$ has all real frequencies at both RHF/ECP and MP2/ECP levels. This structure is higher in energy than the C_{2v} structure by 25.5 kcal/mol (RHF/ECP, basis III). Our finding concerning the existence of the PH_4^- minimum of T_d symmetry agrees with the recent MP2/6-31++G(d,p) result of Ortiz.[9]

Unlike $PH_4^-(T_d)$, the T_d minimum of AsH_4^- did not "survive" after inclusion of electron correlation (Figure 1). That is, a frequency analysis shows that $AsH_4^-(T_d)$ is a local minimum at the RHF/ECP computational level but not at the MP2/ECP level, where a t_2 degenerate vibrational mode has an imaginary frequency and destroys AsH_4^-.

The T_d geometries of SbH_4^- and BiH_4^- are also not stable, regardless of whether the RHF or MP2 method is used. Similarly, any $XF_4^-(T_d)$ structure (Figure 2) is not stable either.

3.3. AE C_{2v} and C_{4v} Optimized Structures—Effect of Electron Correlation on the $XH_4^-(C_{2v})$ and $XH_4^-(C_{4v})$ Structures. In the proceeding section we reported the case of $PH_4^-(C_{2v})$, whose structural stability depended on the inclusion of electron correlation. In this section we present results of systematic AE *ab initio* studies of the correlation effects on the C_{2v} and C_{4v} structures of XH_4^- for X = P, As, and Sb. Also, by the AE calculations, we want to check if the previously revealed periodic trends in the energy differences between the two types of structures (for both the hydrides and fluorides) are not artifacts of the ECP model.

Comparison of Figures 3 and 4 (including AE results obtained using basis AE) with Figures 1 and 2 shows that a satisfactory agreement exists between the AE and ECP geometries and

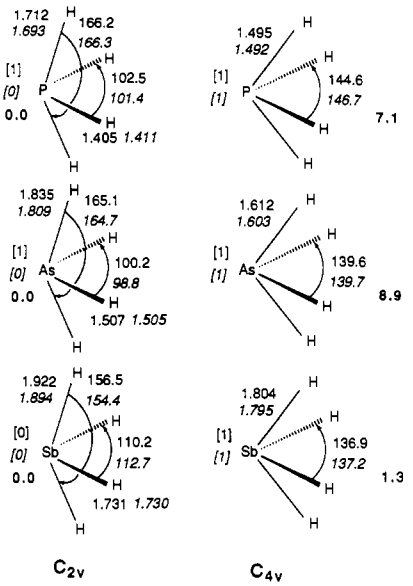

Figure 3. C_{2v} and C_{4v} structures of XH_4^- (X = P, As, Sb) optimized at the RHF and MP2 levels using basis AE (bond lengths in angstroms; bond angles in degrees). Values shown in boldface correspond to RHF energies relative to the C_{2v} structures (in kcal/mol); the number of associated imaginary frequencies is given in square brackets. Values in italics are from the MP2 calculation.

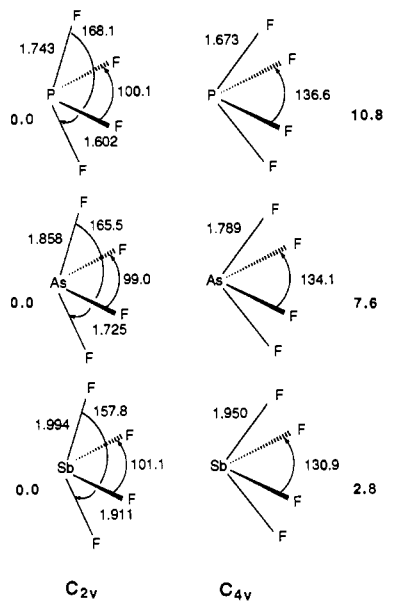

Figure 4. C_{2v} and C_{4v} structures of XF_4^- (X = P, As, Sb) optimized at the RHF level using basis AE (bond lengths in angstroms; bond angles in degrees). Values shown in boldface correspond to RHF energies relative to the C_{2v} structures (in kcal/mol).

corresponding relative energies for both the hydrides and fluorides. In particular, the AE calculations confirm the ECP behavior in the $E(C_{4v}) - E(C_{2v})$ relative energies on passing from X = P to X = As to X = Sb (for the respective MP2/basis AE energy differences of the hydrides; cf. Table 3). The largest discrepancy between the AE and ECP bond angles is seen for $SbH_4^-(C_{2v})$; i.e., the AE structure is more distorted toward the C_{4v} geometry as compared with the ECP finding. The possible source of this discrepancy is that the PES of $SbH_4^-(C_{2v})$ is rather flat along the pseudorotation mode (Scheme 1), as judged by the very small energy difference between the C_{4v} and C_{2v} forms (1.3 kcal/mol at RHF/basis AE). This is even better seen when the energies of the MP2 optimized structures are compared (Table 3), the respective difference become smaller, being only 0.6 kcal/mol.

Vibrational analysis indicates (Figure 3) that $PH_4^-(C_{2v})$ is not structurally stable at the RHF level: the optimized structure is a local minimum only when correlation effects (MP2) are included. Thus, the AE prediction for $PH_4^-(C_{2v})$ is in agreement with the ECP finding for this structure. In contrast to the RHF/ECP result we have found that $AsH_4^-(C_{2v})$ is not structurally stable at the SCF level. According to the AE calculations, the $AsH_4^-(C_{2v})$ structure shows the same behavior as $PH_4^-(C_{2v})$. That is, $AsH_4^-(C_{2v})$ has one imaginary frequency (b_2 mode) and zero imaginary frequencies when the computational method is changed from RHF to MP2, respectively. Apparently, electron correlation effects which strengthen the axial bonds (the MP2 axial bonds of XH_4^- are shorter than the corresponding RHF bonds; Figure 3) stabilize the C_{2v} structures of both PH_4^- and AsH_4^-. On the other hand, electron correlation does not affect the curvature of the PES for the $XH_4^-(C_{4v})$ structures, which are found consistently to be saddle points for pseudorotation.

3.4. RHF/ECP Natural Charges of XH_4^- and XF_4^-. In Table 4 the RHF/ECP charges for the C_{2v}, C_{4v} and D_{4h} optimized structures obtained by using the natural population analysis (NPA)[30] are reported. As Table 4 shows, C_{2v} structures of the fluorides are characterized by much larger charge separation between the central atom and the ligands than the hydrides counterparts. This is in agreement with the larger electronegativity of F as compared to H.[34] These charge separations increase in going down the column. For $XH_4^-(C_{2v})$, the axial hydrogens are much more negatively charged than the equatorial ones, which is consistent with the much longer (and weaker) axial bonds in comparison with the equatorial bonds. For $XF_4^-(C_{2v})$, where the dissimilarity in the bonds is less pronounced than for the corresponding hydrides, the negative charges on the axial and equatorial ligands are more similar. During the C_{2v}–C_{4v} pseudorotation, the polarity of the axial ligands-central atom bond decreases (in $PH_4^-(C_{4v})$ the negative charge reside on both P and H). The C_{4v}–D_{4h} distortion (hydrides) also results in significant reduction of the net negative charge on the ligands.

3.5. Thermodynamic Stabilities. Table 5 shows the change in energies of the reactions: (1) $XH_3 + H^- \rightarrow XH_4^-$, (2) $XF_3 + F^- \rightarrow XF_4^-$, and (3) $XH_2^- + H_2 \rightarrow XH_4^-$, as X is varied. These energies were found from the RHF/ECP and MPn/ECP calculations. For reaction 1, the MP2/basis AE reaction energies with X = P, As, and Sb are also included. It appears from Table 5 that the XH_4^- (XF_4^-) stabilities relative to $XH_3 + H^-$ ($XF_3 + F^-$) increase in the order X = P < X = As < X = Sb ~ X = Bi. We will clarify below this trend by EDA. The XF_4^- anions are much more stable with respect to F^- dissociation than the corresponding XH_4^- anions with respect to H^- dissociation. Electron correlation appreciably stabilizes the XH_4^- anions with X = P and As. This is consistent with the AE vibrational analysis of $PH_4^-(C_{2v})$ and $AsH_4^-(C_{2v})$ where we saw that inclusion of electron correlation changed the nature of the optimized structures from unstable transition states to stable minima. The negative of the values for the reactions 1 and 2 (Table 5) represent the hydride (fluoride) affinities for XH_3 (XF_3). The RHF/ECP fluoride affinity for PF_3 of 43.3 kcal/mol is in good agreement with the SCF value of 45.1 kcal/mol obtained by O'Keeffe.[10]

Unlike reactions 1 and 2, reaction 3 is endothermic for all X (Table 5). In other words, the $XH_4^-(C_{2v})$ species are thermodynamically unstable relative to $XH_2^-(C_{2v}) + H_2$ by at least 30 kcal/mol at the MP4/ECP level. The periodic trend in the XH_4^- stabilities with respect to H_2 loss is not regular; however, the changes in the corresponding MP4/ECP reaction energies along the series are within 3 kcal/mol (Table 5).

3.6. Electronic Stabilities. In addition to the structural and thermodynamic stabilities of any experimentally unknown species, their electronic stabilities should be tested as well,[46] especially for anions. For all the hypervalent anion structures studied, the corresponding energies of the highest occupied molecular orbitals were negative. More detailed examination of the electronic stability of $XH_4^-(C_{2v})$ and $XF_4^-(C_{2v})$ was done by performing UMP2/ECP calculations with basis II on the XH_4 and XF_4 neutrals at the $XH_4^-(C_{2v})$ and $XF_4^-(C_{2v})$ geometries, respectively.[35] At this computational level, the $XH_4^-(C_{2v})$ anions are more stable

Table 4. Natural Net Charges for the C_{2v}, C_{4v}, and D_{4h} Structures of XH_4^- and for the C_{2v} and C_{4v} Structures of XF_4^- (X = P, As, Sb, Bi) from RHF/ECP Calculations[a]

species	Q(X)	Q(H)[b]	Q(H)[c]	species	Q(X)	Q(F)[b]	Q(F)[c]
$PH_4^-(C_{2v})$	+0.131	−0.444	−0.122	$PF_4^-(C_{2v})$	+1.887	−0.768	−0.675
$AsH_4^-(C_{2v})$	+0.286	−0.481	−0.162	$AsF_4^-(C_{2v})$	+2.023	−0.797	−0.714
$SbH_4^-(C_{2v})$	+0.563	−0.510	−0.271	$SbF_4^-(C_{2v})$	+2.219	−0.834	−0.776
$BiH_4^-(C_{2v})$	+0.654	−0.563	−0.263	$BiF_4^-(C_{2v})$	+2.295	−0.858	−0.790
$PH_4^-(C_{4v})$	−0.025	−0.244		$PF_4^-(C_{4v})$	+1.843	−0.711	
$AsH_4^-(C_{4v})$	+0.162	−0.291		$AsF_4^-(C_{4v})$	+1.984	−0.746	
$SbH_4^-(C_{4v})$	+0.482	−0.371		$SbF_4^-(C_{4v})$	+2.191	−0.798	
$BiH_4^-(C_{4v})$	+0.562	−0.390		$BiF_4^-(C_{4v})$	+2.257	−0.814	
$PH_4^-(D_{4h})$	−0.265	−0.184					
$AsH_4^-(D_{4h})$	−0.165	−0.209					
$SbH_4^-(D_{4h})$	+0.100	−0.275					
$BiH_4^-(D_{4h})$	−0.005	−0.249					

[a] Basis II and basis IV were used for the hydrides and fluorides, respectively, and the optimized structures shown in Figures 1 and 2 were assumed. [b] In the case of C_{2v} structure, this stands for the charge on the axial ligand. [c] In the case of C_{2v} structure, this stands for the charge on the equatorial ligand.

Table 5. Energies of the Reactions $XH_3 + H^- \rightarrow XH_4^-$, $XF_3 + F^- \rightarrow XF_4^-$, and $XH_2^- + H_2 \rightarrow XH_4^-$ (X = P, As, Sb, Bi)[a]

reaction	RHF/ECP	MPn/ECP[b]	MP2/AE[c]
$PH_3 + H^- \rightarrow PH_4^-$	3.3[d]	−5.8[d]	−6.2
$AsH_3 + H^- \rightarrow AsH_4^-$	−3.6	−11.4	−10.1
$SbH_3 + H^- \rightarrow SbH_4^-$	−19.2	−24.0	−27.5
$BiH_3 + H^- \rightarrow BiH_4^-$	−19.5	−23.6	
$PF_3 + F^- \rightarrow PF_4^-$	−43.3	−48.6	
$AsF_3 + F^- \rightarrow AsF_4^-$	−55.5	−58.8	
$SbF_3 + F^- \rightarrow SbF_4^-$	−69.4	−69.7	
$BiF_3 + F^- \rightarrow BiF_4^-$	−69.4	−70.4	
$PH_2^- + H_2 \rightarrow PH_4^-$	32.8	30.2	
$AsH_2^- + H_2 \rightarrow AsH_4^-$	35.8	32.9	
$SbH_2^- + H_2 \rightarrow SbH_4^-$	32.2	30.6	
$BiH_2^- + H_2 \rightarrow BiH_4^-$	35.9	33.6	

[a] In kcal/mol. A negative (positive) sign indicates a stabilization (destabilization) of XH_4^- relative to $XH_3 + H^-$ or $XH_2^- + H_2$ and XF_4^- relative to $XF_3 + F^-$. [b] MP4 for the hydrides and MP2 for the fluorides, calculated using basis II at the RHF/ECP geometries. The RHF/ECP (basis II) geometries of $XH_2^-(C_{2v})$ are (the first entry is the bond length in Å, the second entry is the bond angle in deg): for $PH_2^-(C_{2v})$, 1.426, 93.9; for $AsH_2^-(C_{2v})$, 1.530, 93.1; for $SbH_2^-(C_{2v})$, 1.722, 92.4; for $BiH_2^-(C_{2v})$, 1.791, 91.7. The bond length of H_2 optimized at the RHF/ECP (basis II) level is 0.737 Å. [c] MP2 basis AE//MP2/basis AE. The MP2/basis AE geometries of XH_3 are (the first entry is the bond length in Å, the second entry is the bond angle in deg): for PH_3, 1.415, 93.7; for AsH_3, 1.508, 92.5; for SbH_3, 1.708, 92.6. [d] $PH_4^-(C_{2v})$ is not structurally stable at the RHF/ECP level.

than the corresponding XH_4 neutrals by 22.4 (1.0), 29.4 (1.3), 38.6 (1.7), and 40.2 (1.7) kcal/mol (eV) for X = P, As, Sb, and Bi, respectively. In turn, the $XF_4^-(C_{2v})$ anions are more stable than the XF_4 neutrals by 93.7 (4.1), 114.0 (4.9), 118.2 (5.1), and 143.2 (6.2) kcal/mol (eV) for X = P, As, Sb, and Bi, respectively. Thus, at the level of theory employed, both $XH_4^-(C_{2v})$ and $XF_4^-(C_{2v})$ are predicted to be stable to loss of an electron for all X. For the two anion series, the electronic stability increases on going down the column; however, it is much more pronounced for the $XF_4^-(C_{2v})$ series for which the estimated vertical ionization potentials are remarkably large (4.1–6.2 eV).

In addition, the "internal" and "external" electronic stabilities[45] of the RHF/ECP wave function of $XH_4^-(C_{2v})$ and $XF_4^-(C_{2v})$[35] were tested by using the methods of Seeger and Pople.[28,45] For all the C_{2v} anion structures in question, no instability of the RHF/ECP wave function with respect to the perturbations considered[45] was detected.

3.7. Assessment of the Possible Existence of XH_4^- and XF_4^- in Terms of Structural and Thermodynamic Stabilities. The few attempts to synthesize the hypervalent PH_4^- hydride in flowing afterglow experiments have been unsuccessful so far.[42] One difficulty in its preparation in the gas phase may arise from the fact that a global minimum on the PES of PH_4^- is a nonhypervalent $PH_2^- - H_2(C_s)$ species.[43] PH_4^- is unique among the hypervalent hydrides studied since in addition to a C_{2v} minimum it has a T_d minimum (the latter also found to be stable to electron loss[9]), and therefore the existence of a T_d double-Rydberg[9] anion is possible. In this respect, PH_4^- resembles NH_4^-, because the latter also possesses a second minimum of T_d symmetry.[9,48] The "heavier" XH_4^- species with X = As, Sb, and Bi do not show a stable T_d minimum. However, their C_{2v} structures do show minima that are more stable both thermodynamically (relative to $XH_3 + H^-$) and electronically compared to $PH_4^-(C_{2v})$. One can therefore deduce that the common difficulty in preparation of the $XH_4^-(C_{2v})$ hydrides may be their thermodynamic instability with respect to $XH_2^- + H_2$, discussed in section 3.5. Theoretical work aiming at the elucidation of the kinetic stabilities of $XH_4^-(C_{2v})$ is in progress.[47]

The $XF_4^-(C_{2v})$ fluorides appear to be good candidates for isolable four-coordinated species, judging from their appreciable thermodynamic stabilities with respect to $XF_3 + F^-$ (Table 5)[49] and electronic stabilities already discussed in section 3.5. Thus, one emerging way for the isolation of XF_4^- could be based on the XF_3 precursor. Due to the strong ionicity of the fluorides (Table 5), their existence in the solid phase is the most likely.

The experimentally known four-coordinated hypervalent radicals PH_4 and PF_4[50] possess one electron less than PH_4^- and PF_4^-, respectively.

4. Discussion

In an effort to more fully understand the periodic trends revealed in the $E(C_{4v}) - E(C_{2v})$ relative energies of XH_4^- (XF_4^-) and their thermodynamic stabilities with respect to $XH_3 + H^-$ ($XF_3 + F^-$) for X = P, As, Sb, and Bi, an energy decomposition analysis[14] was applied at the RHF/ECP level. In the EDA method, the molecular system, "supermolecule", is considered as composed of two interacting subsystems. The XL_4^- (L = H, F) hypervalent "supermolecules" were considered here as composed of XL_3 and L^- interacting "subsystems", XL_3–L^-.

In order to clarify the trend in the $XL_4^-(C_{2v})$ thermodynamic stabilities, the C_{2v} species were represented by the XL_3–L_{ax}^-

(45) Seeger, R.; Pople, J. A. *J. Chem. Phys.* **1977**, *66*, 3045.
(46) For a comparison of different types of molecular stability, see: Ewig, C. S.; Van Wazer, J. R. *J. Am. Chem. Soc.* **1990**, *112*, 109 and references cited therein.
(47) Moc, J.; Morokuma, K. Unpublished results.
(48) The NH_4^- species was observed recently in the photoelectron experiments: Coe, J. V.; Snodgrass, J. T.; Freidhoff, C. B.; McHugh, K. M.; Bowen, K. H. *J. Chem. Phys.* **1985**, *83*, 3169.
(49) The necessity of diagnosing the relativistic effects for the elucidation of the periodic trends was suggested by a reviewer.
(50) For PH_4, see e.g.: McDowell, C. A.; Mitchell, K. A. R.; Raghunathan, P. *J. Chem. Phys.* **1972**, *57*, 1699. For PF_4, see e.g.: Nelson, W.; Jackel, G.; Gordy, W. *J. Chem. Phys.* **1970**, *52*, 4572.
(51) Schwerdtfeger, P.; Health, G. A.; Dolg, M.; Bennett, M. A. *J. Am. Chem. Soc.* **1992**, *114*, 7518.

Chart 1. $XL_4^-(C_{2v})$ (X = P, As, Sb, Bi; L = H, F) Represented by the XL_3–L_{ax}^- Interacting "Subsystems"[a]

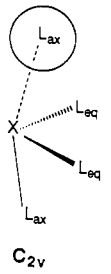

C_{2v}

[a] The L_{ax}^- "subsystem" is indicated by a circle (subscripts "ax" and "eq" denote axial and equatorial, respectively).

Chart 2. $XL_4^-(C_{2v})$ (X = P, As, Sb, Bi; L = H, F) Represented by the XL_3–L_{eq}^- and XL_3–L_{ax}^- Interacting "Subsystems" and $XL_4^-(C_{4v})$ Represented by the XL_3–L^- Interacting "Subsystems"[a]

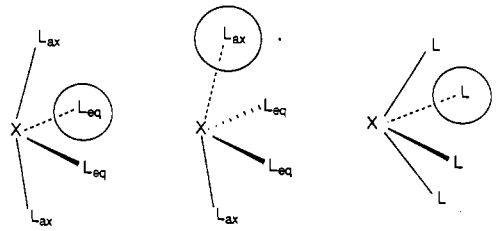

C_{2v} C_{2v} C_{4v}

[a] The L_{eq}^-, L_{ax}^-, and L^- "subsystems" are indicated by circles (subscripts "ax" and "eq" denote axial and equatorial, respectively).

"supermolecules" ($L^- = L_{ax}^-$, Chart 1). This representation is justified for this purpose, as the interaction between the XL_3 and L_{ax}^- "subsystems" through longer(weaker) axial bonds, broken first during L^- dissociation from XL_4^-, will differentiate C_{2v} species with different X.

On the other hand, trying to understand the irregular trend in the $E(C_{4v}) - E(C_{2v})$ energy differences of XL_4^-, we claim that the interaction through shorter (stronger) equatorial bonds will differentiate C_{2v} species with different X and the corresponding relative energies. This is especially true for XH_4^- (C_{2v}), where, as we already mentioned, the difference between the axial and equatorial bonds is appreciable. So, for this purpose, the C_{2v} species were represented by the XL_3–L_{eq}^- "supermolecules" ($L^- = L_{eq}^-$, Chart 2); for comparison, the XL_3–L_{ax}^- "supermolecules" were also considered. For the C_{4v} species, the axial and equatorial positions of L^- are of course equivalent (cf. Chart 2).

In the EDA method,[14] the binding energy, ΔE, the energy difference between the XL_4^- "supermolecule" and the isolated XL_3 and L^- fragments is divided into two parts: the deformation energy, DEF, and the interaction energy, INT:

$$\Delta E = E(XL_4^-) - [E(XL_3, \text{equilibrium}) + E(L^-)] = \text{DEF} + \text{INT}$$

DEF is the energy needed to distort XL_3 from its equilbrium (C_{3v}) structure to the C_s structure it takes in the XL_4^- species:

$$\text{DEF} = E(XL_3, \text{distorted}) - E(XL_3, \text{equilibrium})$$

INT is the energy which comes from the interaction of the distorted XL_3 with L^-:

$$\text{INT} = E(XL_4^-) - [E(XL_3, \text{distorted}) + E(L^-)]$$

The INT energy can be decomposed further into five terms:

$$\text{INT} = \text{ES} + \text{EX} + \text{CTPLX}(L^- \rightarrow XL_3) + \text{CTPLX}(XL_3 \rightarrow L^-) + R$$

where ES is the electrostatic interaction, EX is the exchange repulsion, $\text{CTPLX}(L^- \rightarrow XL_3)$ is the donative interaction from L^- to XL_3, $\text{CTPLX}(XL_3 \rightarrow L^-)$ is the back-donative interaction from XL_3 to L^-, and R is the leftover term. We denoted here INT energies for the C_{2v} and C_{4v} structures INT(C_{2v}) and INT(C_{4v}), respectively, and DEF energies for the C_{2v} and C_{4v} forms as DEF(C_{2v}) and DEF(C_{4v}), respectively.

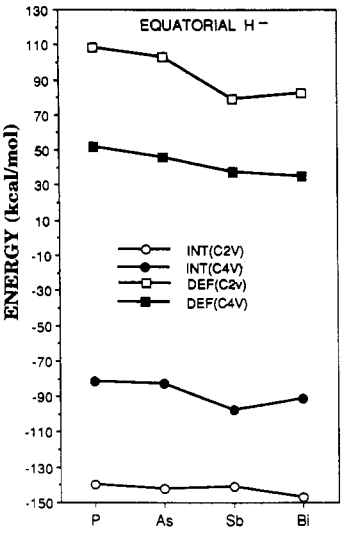

Figure 5. Graphic representation of the INT(C_{2v}), INT(C_{4v}), DEF(C_{2v}), and DEF(C_{4v}) energies of XH_4^- as functions of the central atom X. INT(C_{2v}) and DEF(C_{2v}) were found by assuming the XH_3–H_{eq}^- representation of the C_{2v} "supermolecules".

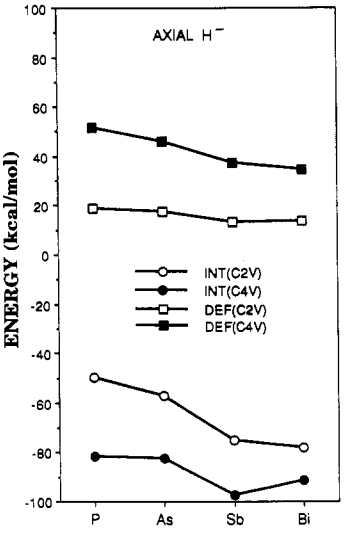

Figure 6. Graphic representation of the INT(C_{2v}), INT(C_{4v}), DEF(C_{2v}), and DEF(C_{4v}) energies of XH_4^- as functions of the central atom X. INT(C_{2v}) and DEF(C_{2v}) were found by assuming the XH_3–H_{ax}^- representation of the C_{2v} "supermolecules".

In Figure 5, INT(C_{2v}) and DEF(C_{2v}) energies found assuming the XH_3–H_{eq}^- "supermolecules" and the INT(C_{4v}) and DEF(C_{4v}) energies of the XH_3–H^- systems were depicted as functions of X. For comparison, in Figure 6, INT(C_{2v}) and DEF(C_{2v}) obtained assuming the XH_3–H_{ax}^- "supermolecules" together with INT(C_{4v}) and DEF(C_{4v}) of the XH_3–H^- systems were also depicted as functions of X (note slightly different energy scales in Figures 5 and 6).

It can be inferred from Figure 5 that, for X = Sb and Bi, the deformation energies for the C_{2v} structures are substantially less positive (less destabilizing) than those for X = P and As, by about 20–30 kcal/mol, DEF(C_{2v}) for X = Sb being the smallest among DEF(C_{2v}) energies. This can be regarded as the first factor (factor 1), geometrical in nature, contributing to the "unexpectedly small" $E(C_{4v}) - E(C_{2v})$ energy difference for SbH_4^-. It can be inferred further from Figure 5 that, for X = Sb, INT(C_{4v}) is more negative (more stabilizing) than expected. In

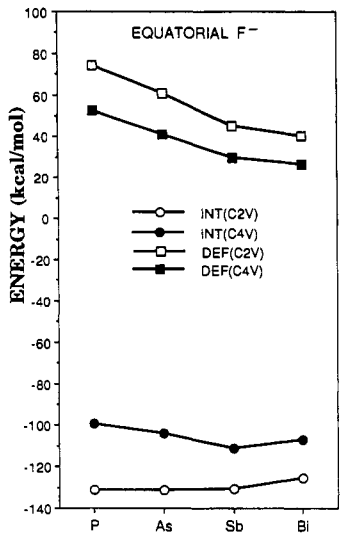

Figure 7. Graphic representation of the INT(C_{2v}), INT(C_{4v}), DEF(C_{2v}) and DEF(C_{4v}) energies of XF_4^- as functions of the central atom X. INT-(C_{2v}) and DEF(C_{2v}) were found by assuming the XF_3–F_{eq}^- representation of the C_{2v} "supermolecules".

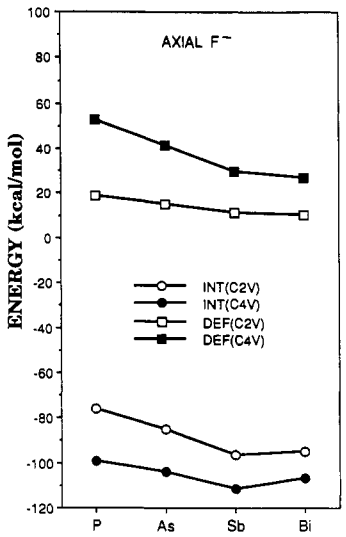

Figure 8. Graphic representation of the INT(C_{2v}), INT(C_{4v}), DEF(C_{2v}) and DEF(C_{4v}) energies of XF_4^- as functions of the central atom X. INT-(C_{2v}) and DEF(C_{2v}) were found by assuming the XF_3–F_{ax}^- representation of the C_{2v} "supermolecules".

particular, this energy is lower by about 15 and 6 kcal/mol than INT(C_{4v}) for X = As and X = Bi, respectively (factor 2). In other words, for SbH_4^-(C_{4v}), the four bonds are stronger than expected from the periodic trend. At the same time (Figure 5), INT(C_{2v}) for X = Sb is less negative (less stabilizing) than expected from the periodic trend. In particular, this energy is higher, by about 6 kcal/mol, than INT(C_{2v}) for X = Bi (factor 3). In other words, for SbH_4^-(C_{2v}), the two equatorial bonds are weaker than expected. Thus, according to Figure 5, the superposition of factors 1–3 results in the relatively small $E(C_{4v})$ – $E(C_{2v})$ energy difference for SbH_4^-, causing the irregular periodic trend in this quantity.

In Figure 7, INT(C_{2v}) and DEF(C_{2v}) energies found assuming the XF_3–F_{eq}^- "supermolecules" and the INT(C_{4v}) and DEF(C_{4v}) energies of the XF_3–F^- systems were depicted as functions of X. For comparison, in Figure 8, INT(C_{2v}) and DEF(C_{2v}) obtained assuming the XF_3–F_{ax}^- "supermolecules" together with INT-(C_{4v}) and DEF(C_{4v}) of the XF_3–F^- systems were also depicted as functions of X.

In contrast to the hydride case, inspection of Figure 7 does not reveal a distinctive factor(s) contributing to the irregularity in the fluorides $E(C_{4v})$ – $E(C_{2v})$ energies, appearing here for X = Sb and Bi (cf. Figure 2). We notice, however, that the difference in these relative energies between SbF_4^- and BiF_4^- is only 1.5 kcal/mol (at RHF/ECP) and is less pronounced than that between the hydride counterparts (5.5 kcal/mol at RHF/ECP). Probably, for the XF_4^- series, a number of factors contribute to the irregularity in question.

Tables 6 and 7 summarize the EDA results including decomposition of INT for XH_4^- and XF_4^-, respectively, obtained assuming the XL_3–L_{ax}^- representation for the C_{2v} structures (Chart 1). The INT and DEF energies from these tables were already used to generate Figures 5–8 (C_{4v} symmetry) and Figures 6 and 8 (C_{2v} symmetry). INT and ΔE energies in Tables 6 and 7 indicate an increase in the stabilization of XH_4^-(C_{2v}) and XF_4^-(C_{2v}) in the order X = P < X = As < X = Sb ~ X = Bi, which is of course consistent with the results of Table 5, showing the periodic trend in the stabilities of XL_4^-(C_{2v}) relative to XL_3 + L^-.[36]

Using the results given in Tables 6 and 7 for the C_{2v} species as a starting point, we will now investigate the origin of this periodic trend by doing an additional energy decomposition analysis. As the trend in the stabilization, i.e. an increase in the order X = P < X = As < X = Sb ~ X = Bi, is similar for the hydrides and fluorides, this additional EDA was done only for the fluorides. Specifically, to clarify intrinsic differences between the XF_4^- species containing different central atoms as represented by the XF_3–F_{ax}^- "supermolecules", a comparison of the INT energy components at the same "interfragment contact" was done. That is, following previous studies,[33] taking the exchange repulsion EX as the measure of contact of electron clouds, for X = P, As, and Sb, we adjusted the F_{ax}^- fragment to central atom distance until the exchange energy matched the exchange energy for BiF_4^-(C_{2v}) (126 kcal/mol). The results of EDA for XF_3–F_{ax}^- with the "common" EX are depicted schematically in Figure 9. Inspection of Figure 9 reveals that the main factor contributing to the stabilization of XF_4^- on passing down the column is the electrostatic interaction, ES. In order to provide additional support for this interpretation, natural charges were computed for the XF_3(C_s) "subsystems" of the XF_4^-(C_{2v}) "supermolecules" (RHF/ECP, basis II). The natural charges on P, As, Sb, and Bi are found to be +1.986, +2.100, +2.286, and +2.321, respectively. Simultaneously (Figure 9), the CTPLX($F^- \rightarrow XF_3$) donative energy is less negative (less stabilizing) for X = Bi than X = Sb (by about 5 kcal/mol) and the back-donative energies

Table 6. Energy Components for the XH_3--H_{ax}^- and XH_3--H^- Interactions within the C_{2v} and C_{4v} Structures of XH_4^-, respectively[a]

	C_{2v} symmetry				C_{4v} symmetry			
	PH_4^-	AsH_4^-	SbH_4^-	BiH_4^-	PH_4^-	AsH_4^-	SbH_4^-	BiH_4^-
ΔE	−31.1	−39.3	−61.8	−64.3	−30.1	−36.6	−60.1	−56.5
DEF	18.8	17.7	13.2	13.6	51.6	46.0	37.5	34.8
INT	−49.9	−57.0	−75.0	−77.9	−81.7	−82.6	−97.6	−91.3
ES	−52.7	−51.5	−57.5	−54.3	−64.8	−65.3	−71.4	−70.6
EX	108.2	84.5	66.1	49.4	160.1	130.2	84.1	78.5
CTPLX[b]	−9.5	−7.9	−8.4	−5.5	−22.9	−17.9	−14.2	−10.8
CTPLX[c]	−95.5	−81.1	−72.9	−62.3	−163.0	−134.9	−97.8	−87.2
R	−0.5	−1.1	−2.3	−5.1	8.8	5.2	1.8	−1.2

[a] RHF/ECP energies (in kcal/mol) calculated with basis I at the RHF/ECP geometries (subscript "ax" denotes axial). A negative (positive) sign indicates stabilization (destabilization). [b] CTPLX($XH_3 \rightarrow H^-$). [c] CTPLX($H^- \rightarrow XH_3$).

Table 7. Energy Components for the XF_3--F_{ax}^- and XF_3--F^- Interactions within the C_{2v} and C_{4v} Structures of XF_4^-, respectively[a]

	C_{2v} symmetry				C_{4v} symmetry			
	PF_4^-	AsF_4^-	SbF_4^-	BiF_4^-	PF_4^-	AsF_4^-	SbF_4^-	BiF_4^-
ΔE	-57.3	-70.2	-85.1	-84.8	-46.3	-62.8	-81.7	-80.2
DEF	18.9	14.9	11.2	10.1	52.8	41.4	29.7	26.8
INT	-76.2	-85.1	-96.3	-94.9	-99.1	-104.1	-111.4	-107.0
ES	-251.3	-210.7	-184.4	-161.2	-278.4	-230.0	-193.4	-170.8
EX	295.9	220.0	164.8	126.4	326.2	238.7	167.4	133.8
CTPLX[b]	-31.2	-25.7	-24.1	-17.0	-38.9	-31.3	-27.9	-20.6
CTPLX[c]	-105.1	-79.8	-62.2	-48.5	-126.5	-94.0	-67.8	-55.0
R	15.4	11.1	9.6	5.3	18.5	12.5	10.3	5.5

[a] RHF/ECP energies (in kcal/mol) calculated with basis I at the RHF/ECP geometries (subscript "ax" denotes axial). A negative (positive) sign indicates stabilization (destabilization). [b] CTPLX($XF_3 \rightarrow F^-$). [c] CTPLX($F^- \rightarrow XF_3$).

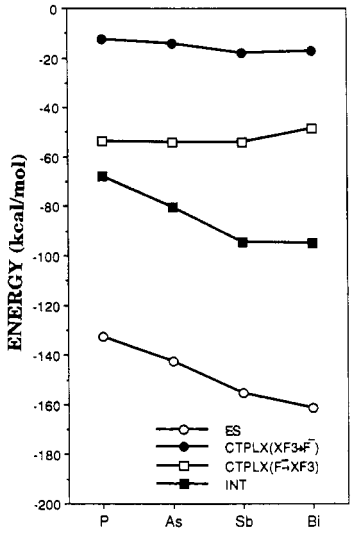

Figure 9. Graphic representation of the INT energy and its components for the XF_3–F_{ax}^- "supermolecules" as functions of the central atom X, obtained at the same "interfragment contact".

CTPLX($XF_3 \rightarrow F^-$) are nearly the same for X = Sb and X = Bi. We thus conclude on the basis of Figure 9 that the ES term influences predominantly the INT behavior on going from X = P to X = As to X = Sb, whereas on passing from X = Sb to X = Bi, the donative CTPLX($F^- \rightarrow XF_3$) energy affects the "shape" of INT in addition to ES.

5. Conclusions

From the *ab initio* ECP and AE results presented and discussed in the previous sections, the following major conclusions emerge.

(i) For both XH_4^- and XF_4^-, the structures of lowest energy among the structures considered were of C_{2v} symmetry (PTBP shape). $SbH_4^-(C_{2v})$ and $BiH_4^-(C_{2v})$ were shown to be minima on both the SCF and MP2 PES. By contrast, the inclusion of electron correlation changed the nature of $PH_4^-(C_{2v})$ and $AsH_4^-(C_{2v})$ from unstable saddle points to stable minima; for the two species, further computations employing higher levels of approximation than MP2 may be needed to confirm their structural stability. All $XF_4^-(C_{2v})$ were found to be minima on the SCF PES.

(ii) D_{4h} structures of XH_4^- and PF_4^- appeared to be transition states for inversion of the C_{4v} structures. On the other hand, C_{4v} structures of XH_4^- and XF_4^- were found to be saddle points connecting C_{2v} minima in the C_{2v}–C_{4v}–C_{2v} pseudorotation. Among the hypervalent hydrides and fluorides studied, only PH_4^- showed a stable minimum with T_d symmetry.

(iii) The periodic trends revealed in the $E(C_{4v}) - E(C_{2v})$ energy differences for both XH_4^- and XF_4^- were irregular. Using the energy decomposition analysis of Morokuma and Kitaura it was pointed out that for the hydride series, relatively strong bonds in $SbH_4^-(C_{4v})$, relatively weak equatorial bonds in $SbH_4^-(C_{2v})$ as well as relatively small deformation energy for the latter species contributed to this irregularity.

(iv) The thermodynamic stabilities of $XH_4^-(C_{2v})$ and $XF_4^-(C_{2v})$ relative to $XH_3(C_{3v}) + H^-$ and $XF_3(C_{3v}) + F^-$, respectively, were found to increase in the order X = P < X = As < X = Sb ~ X = Bi. The increasing electrostatic interaction ES between the XF_3 and F^- "subunits" was pointed out by EDA to be the main origin of this periodic behavior for the XF_4^- species represented by the XF_3–F_{ax}^- "supermolecules".

(v) All the $XH_4^-(C_{2v})$ hydrides were shown to be thermodynamically unstable with respect to H_2 loss by about 30 kcal/mol at the MP4/ECP level.

(vi) For X = P, As, and Sb, the ECP predictions with regard to the optimized geometries, relative energies, and periodic trends were in a full agreement with the all-electron findings obtained using basis AE and 6-31+G(d) basis sets.

Finally, we have predicted here periodic trends in the geometries and relative energies for the group 15 hypervalent species and illustrated three cases in terms of EDA. It is likely that some of the trends revealed are influenced by the relativistic contributions from the "heavy" species.[49] The major relativisitic effects for the Sb and Bi elements (but not for P and As) were incorporated into the ECP's we used.[4d] However, in order to examine the influence of the relativistic effects on a given molecular property it is necessary to compare results of relativistic (R) and nonrelativistic (NR) calculations on that property (see, e.g., ref 52). We believe that an analysis of this type provides more insight into the periodic trends revealed and discussed in this work. Examples of the comparative NR and R calculations on the group 15 compounds can be found in the recent literature.[41,51]

Acknowledgment. J.M. would like to acknowledge the Japan Society for the Promotion of Science for a postdoctoral fellowship. He also thanks Drs. N. Koga and J. Anchell for helpful discussions, Mr. T. Komatsuzaki for his version of EDA program, and Mr. N. Matsunaga for communication of unpublished results. Part of the calculation was carried out at the IMS Computer Center.

Supplementary Material Available: Tables giving a complete set of total energies obtained from both ECP and AE calculations (6 pages). Ordering information is given on any current masthead page.

(52) Kaupp, M.; Schleyer, P. v. R. *J. Am. Chem. Soc.* **1993**, *115*, 1061 and references cited therein.